

Metal–metal bonding using silver/copper nanoparticles

Y. Kobayashi¹ · T. Maeda¹ · Y. Yasuda² · T. Morita²

Received: 29 June 2015 / Accepted: 5 August 2015 / Published online: 19 August 2015
© The Author(s) 2015. This article is published with open access at Springerlink.com

Abstract A method for producing nanoparticles composed of silver and copper and a metal–metal bonding technique using the silver/copper nanoparticles are proposed. The method consists of three steps. First, copper oxide nanoparticles are produced by mixing $\text{Cu}(\text{NO}_3)_2$ aqueous solution and NaOH aqueous solution. Second, copper metal nanoparticles are fabricated by reducing the copper oxide nanoparticles with hydrazine in the presence of poly(vinylpyrrolidone) (PVP). Third, silver/copper nanoparticles are synthesized by reducing Ag^+ ions with hydrazine in the presence of the copper metal nanoparticles. Initial concentrations in the final silver/copper particle colloid, composed of 0.0075 M Cu^{2+} , 0.0025 M Ag^+ , 1.0 g/L PVP, and 0.6 M hydrazine, produced silver/copper nanoparticles with an average size of 49 nm and a crystal size of 16.8 nm. Discs of copper metal were successfully bonded by the silver/copper nanoparticles under annealing at 400 °C and pressurizing at 1.2 MPa for 5 min in not only hydrogen gas but also nitrogen gas. The shear force required to separate the bonded discs was 22.3 MPa for the hydrogen gas annealing and 14.9 MPa for the nitrogen gas annealing (namely, 66.8 % of that for hydrogen gas annealing).

Keywords Nanoparticles · Copper · Silver · Filler · Metal–metal bonding

✉ Y. Kobayashi
ykoba@mx.ibaraki.ac.jp

¹ Department of Biomolecular Functional Engineering,
College of Engineering, Ibaraki University, 4-12-1
Naka-narusawa-cho, Hitachi, Ibaraki 316-8511, Japan

² Hitachi Research Laboratory, Hitachi Ltd, 7-1-1 Omika-cho,
Hitachi, Ibaraki 319-1292, Japan

Introduction

Metal–metal bonding is an important process in fields such as electronics, metalworking, structural materials, and materials science (Guo et al. 2015; Tyler 2015). Solder, aka filler, is often used in various metal–metal bonding processes (mainly in the field of electronics). Alloys composed mainly of lead and tin are representative fillers used in conventional solder-based bonding techniques (Basaran and Jiang 2002; Gomez and Basaran 2006; Iqbal et al. 2014). They have low melting points, so they can bond materials to be bonded at low energy with no thermal damage to the joints. Since lead is a harmful material (Chen et al. 2015; Rödel et al. 2015), its use tends to be limited. Accordingly, most fillers should be lead free. As lead-free fillers, tin-based alloys have been developed (Lu et al. 2014; Kotadia et al. 2014; Yu et al. 2014; Belyakov and Gourlay 2015). However, these alloys have low melting points, so they remelt at relatively low temperatures (above their melting point), thereby breaking the joints they form.

Apart from lead-based alloy and tin-based alloy, metallic materials such as gold, silver, and copper are candidates as fillers, because of their high electrical conductivity and thermal conductivity. However, metal–metal bonding with such metallic fillers requires annealing at high temperature, because their melting points are significantly higher than those of conventional lead-based and tin-based fillers. This annealing causes exposure of the metallic fillers present in the joints to the high temperature during the bonding, thereby damaging the joints thermally.

Nanoparticles of metals solve the problem related to their melting point, since their melting point decreases as their size decreases (Das and Ghosh 2015; Sun et al. 2015); consequently, metal–metal bonding can be performed at

low temperatures. Bonding using metal nanoparticles has another advantage: the nanoparticles become metal bulk after the bonding. The metal bulk should have a melting point higher than that of the nanoparticles. As a result, the bonded materials do not separate when used below their melting points. From this viewpoint, nanoparticles of various metal have been examined with the aim of applying them to bonding (Li et al. 2014; Daly et al. 2015). Silver metal nanoparticles (silver nanoparticles) have been intensively focused on, because silver metal is electrically and thermally conductive as well as being chemically stable. Though silver nanoparticles achieve adequate bonding, the bonding process using the silver nanoparticles faces problems of high cost and ionic migration of silver atoms.

Copper metal nanoparticles (copper nanoparticles) are also a candidate for metal nanoparticle filler, because copper metal does not incur great cost and is superior in terms of anti-ionic migration to silver metal. However, copper nanoparticles are easily oxidized in air (Park et al. 2007; Kanninen et al. 2008), thereby spoiling bonding properties. To solve that problem, our research group previously developed methods for fabricating chemically stable copper metal particles. That is, the particles were produced by reducing Cu^{2+} (Kobayashi et al. 2012, 2013a) or copper oxide nanoparticles (Maeda et al. 2012; Kobayashi et al. 2014) in aqueous solution in the presence of stabilizer. The fabricated copper particles had excellent metal–metal bonding ability. The bonding was performed in a reducing atmosphere to prevent the copper particles from being oxidized. Concerning safety, the use of a reducing atmosphere makes the bonding process complicated. Accordingly, from the viewpoint of a safe bonding process, atmospheres such as air and nitrogen gas are preferable.

As for metal–metal bonding using silver nanoparticles, the process does not always use a reducing atmosphere. Successful bonding is achieved thanks to the chemical stability of silver metal. It can thus be expected that nanoparticles composed of copper particles and silver particles can be used as a new nanoparticle filler for metal–metal bonding in a non-reducing atmosphere without the effect of ionic migration.

In the present work, a method for producing silver/copper nanoparticles for metal–metal bonding is proposed. The nanoparticles are prepared by reducing CuO nanoparticles to copper nanoparticles, and then reducing Ag^+ ions in the presence of the copper nanoparticles in aqueous solution. Their bonding properties in atmospheres such as hydrogen gas and nitrogen gas were also studied.

Experimental

Materials

Copper (II) nitrate trihydrate ($\text{Cu}(\text{NO}_3)_2 \cdot 3\text{H}_2\text{O}$) [77.0–80.0 %, as $\text{Cu}(\text{NO}_3)_2$] and sodium hydroxide solution (NaOH) were used as CuO precursors. Silver nitrate (AgNO_3) (>99.8 %) was used as precursors of silver. Polyvinylpyrrolidone (PVP) [K-30 (Mw = 4000)] was used as a dispersing agent in preparation of nanoparticles. Hydrazine monohydrate (>98.0 %) was used as a reducing reagent for metal ions. All chemicals were purchased from Kanto Chemical Co., Inc., and were used as received. Water that was ion-exchanged and distilled with Yamato WG250 was used in all the preparations, and it was deaerated by bubbling with nitrogen gas for 30 min prior to prepare aqueous solutions.

Preparation

A silver/copper nanoparticle colloid was prepared by the following procedure: (1) production of copper oxide nanoparticles, (2) reduction of the copper oxide to copper metal, and (3) reduction of Ag^+ ions in the presence of copper nanoparticles. In the first step, the copper oxide nanoparticle colloid was prepared by metal salt–base reaction. An aqueous solution of NaOH was added to $\text{Cu}(\text{NO}_3)_2$ aqueous solution under vigorous stirring at 80 °C. Initial concentrations of Cu^{2+} and NaOH in the final copper oxide nanoparticle colloid were 0.010 and 0.019 M, respectively. The reaction time was 3 h. In the second step, the copper nanoparticle colloid was prepared by adding an aqueous solution of PVP and hydrazine in turn to the copper oxide nanoparticle colloid under vigorous stirring at 40 °C. Initial concentrations of Cu^{2+} ions, hydrazine, and PVP in the final copper nanoparticle colloid were 0.9375, 0.5625 M, and 1.25 g/L, respectively. The reaction time was 15 min. The silver/copper nanoparticle colloid solution was obtained in the third step. An aqueous solution of AgNO_3 and hydrazine was added to the as-prepared copper nanoparticle colloid under vigorous stirring at 40 °C, and the vessel containing the colloid was shaded with aluminum foil. Silver content in the silver/copper nanoparticle colloid was adjusted to 0, 25, 50, 75, and 100 mol % by varying the amounts of copper nanoparticle colloid and aqueous solution of AgNO_3 . The silver/copper nanoparticles with the silver contents were indicated as $\text{Ag}_0\text{Cu}_{100}$ (i.e., copper), $\text{Ag}_{25}\text{Cu}_{75}$, $\text{Ag}_{50}\text{Cu}_{50}$, $\text{Ag}_{75}\text{Cu}_{25}$, and $\text{Ag}_{100}\text{Cu}_0$ (i.e., silver), respectively. Initial concentrations of metal ($\text{Cu}^{2+} + \text{Ag}^+$), hydrazine, and PVP in the final silver/copper nanoparticle colloid were 0.01 M, 0.6 M (total

hydrazine concentration), and 1.0 g/L, respectively. The reaction time was 165 min.

Characterization

The nanoparticles were characterized by transmission electron microscopy (TEM), X-ray diffractometry (XRD), and X-ray photoelectron spectroscopy (XPS). TEM was performed with a JEOL JEM-2100 microscope operating at 200 kV. Samples for TEM were prepared by dropping and evaporating the particle colloid on a collodion-coated molybdenum grid. XRD measurements were carried out with a Rigaku Ultima IV X-ray diffractometer at 40 kV and 30 mA with $\text{CuK}\alpha_1$ radiation. For preparing powder samples for the XRD measurements, the supernatant of the particle colloid was removed with decantation, and then residue of the colloid solution was dried at room temperature for 24 h in vacuum. The XPS spectra were obtained using a JEOL JPS-9010 equipped with a monochromatic Mg $\text{K}\alpha$ radiation source (200 W, 10 kV, 1253.6 eV). The XPS samples were the same as the XRD samples. To study the composition below the surface of the powder samples, the particles were etched using 500-kV Ar^+ -ion sputtering. To clean the surface of the nanoparticles, etching was performed once prior to the main measurements.

The bonding property of the fabricated nanoparticles was investigated with the same set-up as used in our previous works (Yasuda et al. 2009; Kobayashi et al. 2011; Maeda et al. 2015). The powder samples, obtained in the same procedure as used for the XRD measurements, were sandwiched between a large copper disc (diameter: 10 mm; thickness: 5 mm) and a small disc (diameter: 5 mm; thickness: 2.5 mm) and pressed under annealing at 400 °C in hydrogen gas or nitrogen gas at 1.2 MPa for 5 min with a Shinko Seiki vacuum reflow system. To examine bonding strength, shear strengths, namely, the force required to separate the bonded plate and stage, were measured with a Seishin SS-100KP bond tester. The disc surfaces were characterized by scanning electron microscopy (SEM) after the shear strengths were measured. SEM was performed with a JEOL JSM-5600LV microscope operating at 15 kV.

Results and discussion

Silver/copper nanoparticles

TEM images of the prepared silver/copper nanoparticles are shown in Fig. 1. All the particles appear somewhat distorted. Figure 2 shows particle size distributions of the particles, which were measured in the TEM images. In all the particles examined, the particle sizes were distributed in a wide range. They are not mono-dispersed. The average

particle sizes were estimated from the distributions. The sizes of the $\text{Ag}_0\text{Cu}_{100}$, $\text{Ag}_{25}\text{Cu}_{75}$, $\text{Ag}_{50}\text{Cu}_{50}$, $\text{Ag}_{75}\text{Cu}_{25}$, and $\text{Ag}_{100}\text{Cu}_0$ nanoparticles are 90 ± 16 , 49 ± 14 , 65 ± 12 , 43 ± 16 , and 65 ± 18 nm, respectively. The nanoparticles containing silver are smaller than the copper nanoparticles (i.e., the nanoparticles containing no silver) and the silver nanoparticles (i.e., the nanoparticles containing no copper). The co-existences of silver ions and copper nanoparticles are considered to control particle growth. The silver ions were present among the nanoparticles, which decreased collision frequency of the nanoparticles. As a result, the particle growth was controlled.

An XRD pattern of the $\text{Ag}_0\text{Cu}_{100}$ nanoparticles is shown in Fig. 3a. Peaks appear clearly at 43.3, 50.4, and 74.1 degrees, and they are attributed to the (110), (111), and (200) reflections of cubic copper (JCPDS card No. 4-0836), respectively. Their average crystal size (14.8 nm) was estimated from X-ray diffraction line broadening of the (111) peak according to the Scherrer equation. The particle size is larger than the crystal size, which indicates that the $\text{Ag}_0\text{Cu}_{100}$ particles are polycrystalline. A slight peak also appears at 36.4 degree, which is assigned to the (111) reflection of cubic Cu_2O (JCPDS card No. 5-0667). XRD patterns of the silver/copper nanoparticles are shown in Fig. 3b–d. Besides the peaks due to cubic copper metal, peaks appear at ca. 38.1, 44.3, 64.4, and 77.5. They are assigned to the (111), (200), (220), and (311) reflections of cubic metallic silver (JCPDS card No. 4-0783), respectively. This result indicates that both Ag^+ and Cu^{2+} ions can be reduced with the present method. The crystal sizes of copper and silver were estimated by applying the Scherrer equation to the (111) cubic metallic copper peak and the (111) cubic metallic silver peak, respectively. The copper crystal sizes for $\text{Ag}_{25}\text{Cu}_{75}$, $\text{Ag}_{50}\text{Cu}_{50}$, and $\text{Ag}_{75}\text{Cu}_{25}$ are 16.8, 14.8, and 13.6 nm, respectively. For silver, the sizes are 11.7, 14.8, and 13.6 nm, respectively. The particle sizes are also larger than the crystal sizes. Accordingly, the $\text{Ag}_{25}\text{Cu}_{75}$ particles, $\text{Ag}_{50}\text{Cu}_{50}$ particles, and the $\text{Ag}_{75}\text{Cu}_{25}$ particles are considered to also be polycrystalline. The copper crystal size of the copper nanoparticles and that of the nanoparticles containing silver are not significantly different. In other words, the co-existence of silver ions does not remarkably affect the copper crystal size. An XRD pattern of the $\text{Ag}_{100}\text{Cu}_0$ nanoparticles is shown in Fig. 3e. Peaks assigned to the (111), (200), (220), and (311) reflections of cubic metallic silver appear at 38.4, 44.3, 64.4, and 77.5, respectively. The silver crystal size was estimated as 23.4 nm. Since the particle size is also larger than the crystal size, the silver particles formed polycrystallite. The silver crystal size of 23.4 nm was larger than those of $\text{Ag}_{25}\text{Cu}_{75}$, $\text{Ag}_{50}\text{Cu}_{50}$, and the $\text{Ag}_{75}\text{Cu}_{25}$. This result indicates that the co-existence of copper particles controls the crystal growth of silver. The TEM observation

Fig. 1 TEM images of silver/copper particles in samples composed of, **a** Ag₀Cu₁₀₀, **b** Ag₂₅Cu₇₅, **c** Ag₅₀Cu₅₀, **d** Ag₇₅Cu₂₅, and **e** Ag₁₀₀Cu₀ nanoparticles

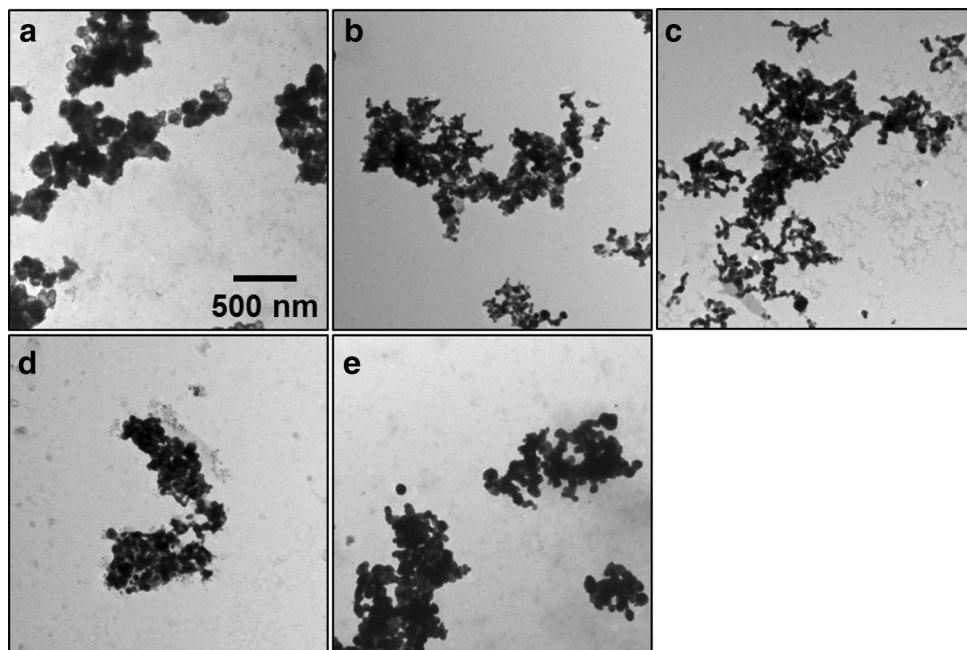
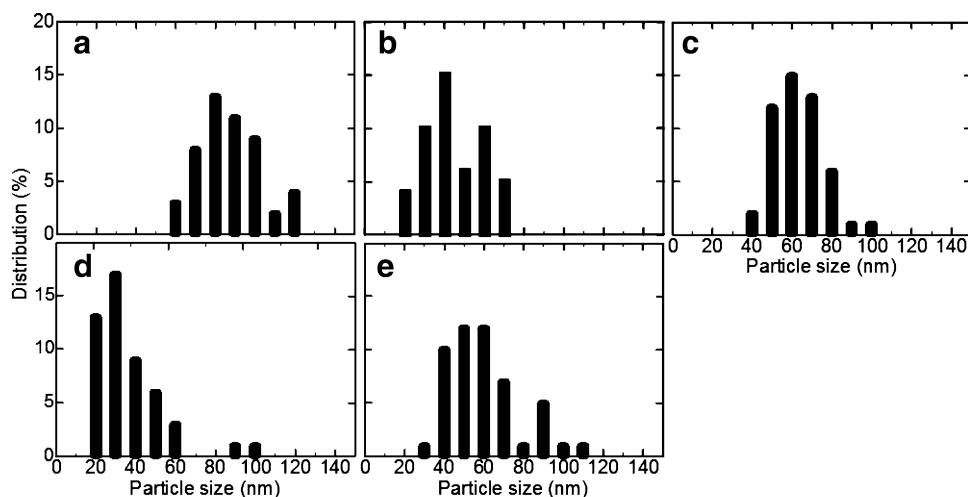


Fig. 2 Particle size distributions of silver/copper particles. The particle sizes were measured in the TEM images. The samples were the same as in Fig. 1



(Fig. 1) suggests that particle growth is controlled by the co-existence of copper particles. The Ag⁺ ions are reduced to form silver metal nuclei, which form silver crystallites and particles directly. In the cases of co-existences of copper particles, the silver nuclei are also deposited on the surface of the copper nanoparticles. This deposition probably prevents the direct formation of silver crystallites and nanoparticles, because of the mismatch between *d* values of silver and copper. As a result, in the case of the nanoparticles containing silver, the growth of silver crystallites and silver nanoparticles is controlled.

The XRD peak position of copper does not shift remarkably with increasing silver content. In contrast, that of silver shifts to a small angle with increasing silver

content. The *d* values of copper and silver in silver/copper nanoparticles are summarized in **Table 1**. The *d* values for copper are almost constant (at ca. 0.2076 nm) in the silver content range of 0–75 mol %: the components of the copper nanoparticles did not change even in co-existence with silver ions. The *d* value for silver tends to increase from 0.2343 to 0.2352 nm with increasing silver content from 25 to 100 mol %: the *d* value became apart from that of copper-free silver nanoparticles with the increase. This tendency indicated that the copper was incorporated into the silver nanoparticles to form silver-rich silver/copper alloy.

Cu 2p_{3/2} XPS spectra of samples of Ag/Cu nanoparticles after several etchings are shown in **Fig. 4**. Each etched

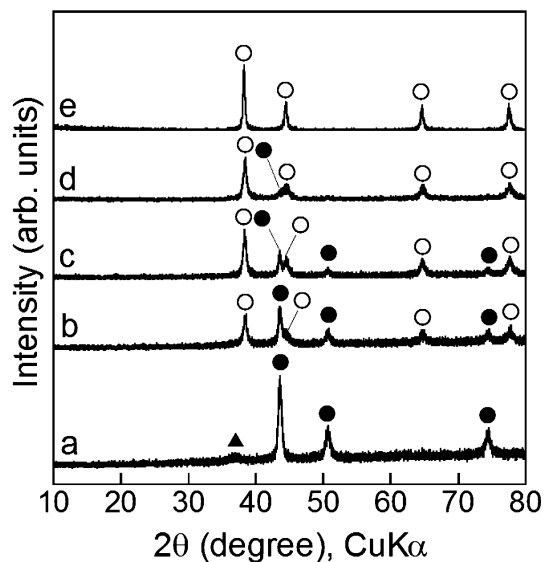


Fig. 3 XRD patterns of silver/copper nanoparticles in samples composed of, *a* Ag₀Cu₁₀₀, *b* Ag₂₅Cu₇₅, *c* Ag₅₀Cu₅₀, *d* Ag₇₅Cu₂₅, and *e* Ag₁₀₀Cu₀ nanoparticles. Filled circle cubic Cu, open circle cubic Ag, filled triangle cubic Cu₂O

sample shows a clear peak. XPS peak position as a function of number of etchings is plotted in Fig. 5. The peak position increases from 932.64 to 932.74 eV as the number of etchings increases from 1 to 5. According to the references (Ghodselahi et al. 2008; Luo et al. 2015), peak positions of (Cu⁺-O/Cu⁰-Cu⁰) and Cu²⁺-O are 932.3–933.8 and 934.5–935.2 eV. It is difficult to distinguish the peak positions of Cu⁺-O and Cu⁰-Cu⁰ because according to XPS analysis, the difference in binding energies of these two bonds is only 0.1–0.2 eV (Mansikkamäki et al. 2006; Ghodselahi et al. 2008; Luo et al. 2015). It has been confirmed by some works performing Auger spectroscopy that the binding energy of Cu⁰-Cu⁰ is higher than that of Cu⁺-O (Ren et al. 2004). Accordingly, the peak position is considered to increase with increasing amount of Cu⁰-Cu⁰. In consideration of the possible assignments of peak positions for these bonds, the XPS spectra were fitted with a Gaussian peak using peak position, peak intensity, and FWHM (full width at half maximum) as fitting parameters. The curve-fitting gave binding energies of 932.5, 932.7, and 933.8 eV. According to the references (Ghodselahi et al. 2008; Plackowski et al. 2013), the order of binding energy is Cu⁺-O < Cu⁰-Cu⁰ < Cu²⁺-O. Thus, these peaks can be assigned to the Cu⁺-O, Cu⁰-Cu⁰, and Cu²⁺-

O bonds, respectively. The XRD measurement revealed no significant peaks due to copper oxide. Accordingly, the species derived from the Cu⁺-O and Cu²⁺-O bonds are speculated to form fine domains, which are too small to be detected by XRD. The intensity of spectrum due to the Cu⁰-Cu⁰ bond became large with the increasing number of etchings. This change in the intensity provided the increase in peak position. Atomic ratios of bonds estimated from the XPS peak area intensity are shown in Fig. 6. Ratios of the Cu⁺-O, Cu⁰-Cu⁰, and Cu²⁺-O bonds decrease, increase, and are almost constant, respectively, as etching time increases. These results indicate that the copper on the surface of the silver/copper nanoparticles is oxidized. Ag 3d_{5/2} XPS spectra of the Ag/Cu nanoparticles after etching are shown in Fig. 7. Each etched sample shows a clear peak. XPS peak position is plotted as a function of number of etchings in Fig. 5. The peak position is 368.04 eV after one etching number, increases to 368.07 eV after two etchings, and almost levels out after two etchings. According to references (Palacio et al. 2003; Gao et al. 2004; Prieto et al. 2012), the peak positions of Ag⁺-O and Ag⁰-Ag⁰ are 374.1 and 368.1 eV, respectively; The order of binding energy is Ag⁺-O > Ag⁰-Ag⁰. The increase and the level-off indicated that the silver contained on the surface of the nanoparticles is slightly oxidized. It is thus concluded from these results that the Ag/Cu nanoparticles are composed of a body of copper and silver and a thin oxide surface.

Metal–metal bonding property

Bonding in hydrogen gas

Photographs of large copper discs after bonding in hydrogen gas and tested to measure their shear strength are shown in Fig. 8. The surfaces of both the copper nanoparticles and the silver/copper nanoparticles are brown. The brown surfaces appear to be derived from the bulk composed of copper metal. These observations imply that the nanoparticles are composed of bulk metal phase with no oxidation and contribute to bonding of the copper discs. Most of the silver nanoparticles are not left on the surface of the Ag₁₀₀Cu₀ nanoparticles, implying that the affinity between the copper disc surface and the silver nanoparticles is weak and contributes little to the bonding. Shear strength is plotted as a function of silver content in

Table 1 *d* values of copper and silver in silver/copper nanoparticles

Ag content (mol %)	0	25	50	75	100
<i>d</i> value for Cu (nm)	0.2076	0.2076	0.2078	0.2075	–
<i>d</i> value for Ag (nm)	–	0.2343	0.2346	0.2343	0.2352

Fig. 4 Cu 2p_{3/2} XPS spectra of silver/copper nanoparticles in a sample composed of Ag₂₅Cu₇₅ nanoparticles. The measured spectra are shown as *black curves* (*black line*). The XPS sample was etched by Ar⁺-ion sputtering; the numbers of etchings were, **a** 1, **b** 2, **c** 3, and **d** 4, **e** 5, and **f** 6. The spectra were fitted with Gaussian peaks due to (*red line*) Cu–Cu, (*blue line*) Cu⁺–O, and (*green line*) Cu²⁺–O bonds

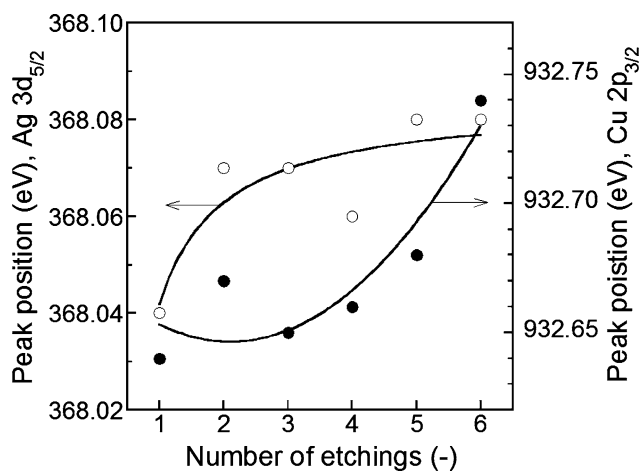
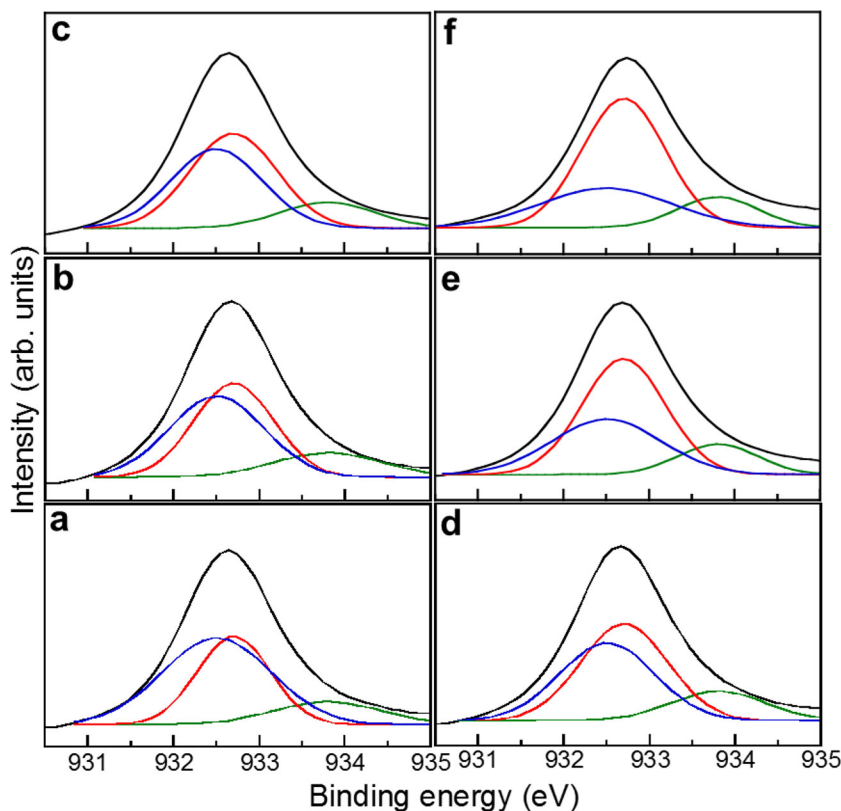


Fig. 5 XPS peak positions vs. number of etchings for silver/copper nanoparticles. The sample was composed of Ag₂₅Cu₇₅ nanoparticles. *Filled circle* Cu, *open circle* Ag

the nanoparticles in Fig. 9 black dots. In the case of all the silver contents, shear strength exceeds 20 MPa, and it tends to decrease slightly with increasing silver content. Since the *d* values of copper and silver do not match, the nanoparticles with large silver contents do not effectively contribute to the bonding of the copper discs. SEM images of the surface of the copper stage after the measurement of shear strength are shown in Fig. 10. Dimples accompanied

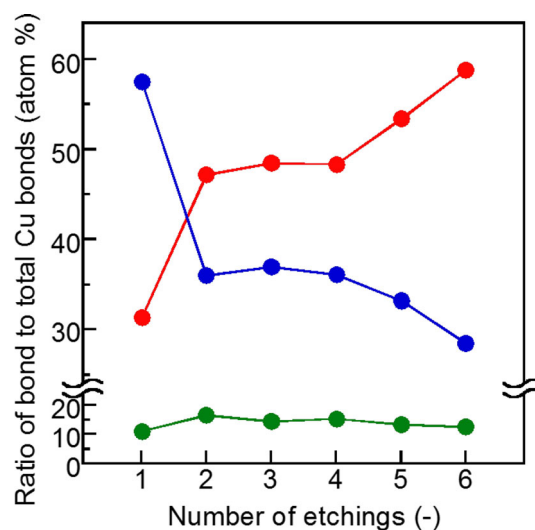


Fig. 6 Atomic ratios of various bonds on the surfaces of the silver/copper nanoparticles as a function of number of argon-ion etching steps. (*Filled red circle*) Cu–Cu, (*filled blue circle*) Cu⁺–O, and (*filled green circle*) Cu²⁺–O. The sample was composed of Ag₂₅Cu₇₅ nanoparticles

with sharp tips appear on the surfaces of the copper discs bonded with the Ag₀Cu₁₀₀ and the Ag₂₅Cu₇₅ nanoparticles. Metallic materials often form such dimples in strongly bonded regions when they are separated with shear stress (Yan et al. 2013; Kobayashi et al. 2013b). These

Fig. 7 Ag 3d_{5/2} XPS spectra of silver/copper nanoparticles. The sample was composed of Ag₂₅Cu₇₅ nanoparticles. The XPS sample was etched by Ar⁺-ion sputtering; the numbers of etchings were, **a** 1, **b** 2, **c** 3, and **d** 4, **e** 5, and **f** 6

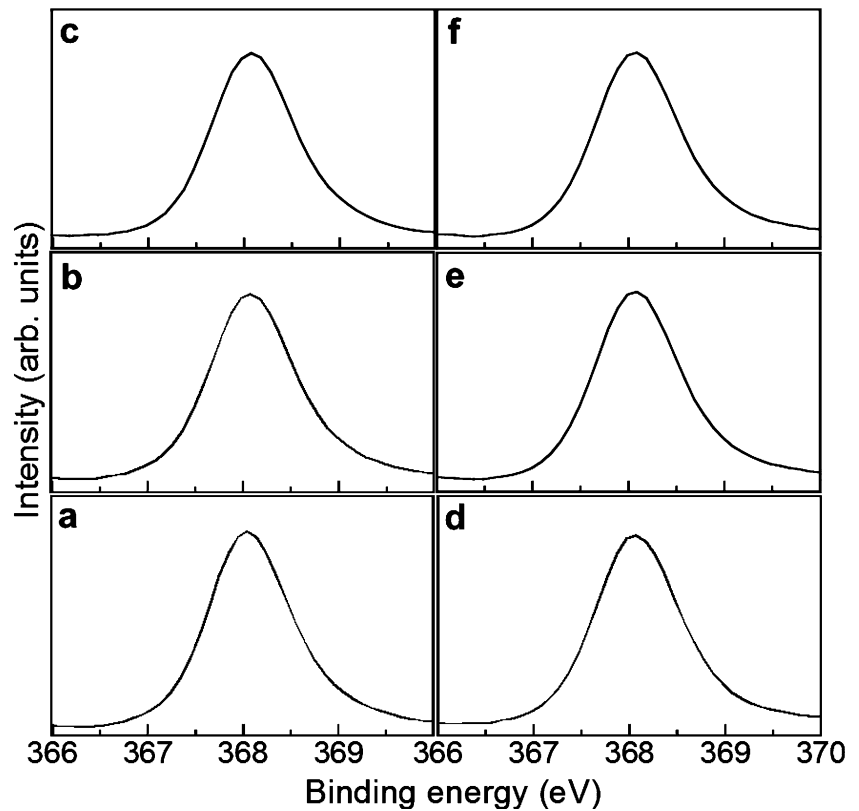
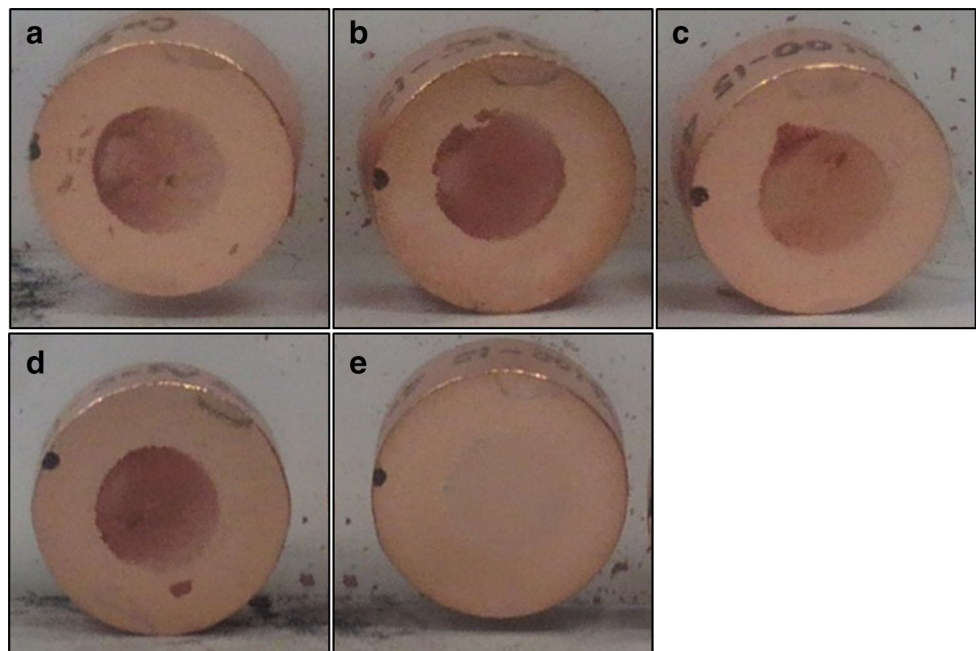


Fig. 8 Photographs of copper plates after measurement of shear strength. The powders used were composed of, **a** Ag₀Cu₁₀₀, **b** Ag₂₅Cu₇₅, **c** Ag₅₀Cu₅₀, **d** Ag₇₅Cu₂₅, and **e** Ag₁₀₀Cu₀ nanoparticles. The bonding was performed in hydrogen gas



observations of dimples support the existence of strong bonding. As for the Ag₅₀Cu₅₀, the Ag₇₅Cu₂₅, and the Ag₁₀₀Cu₀ nanoparticles, dimples were not clearly observed. Sintering among the nanoparticles appeared to

take place. It is considered to contribute to the bonding, although the shear strengths of these bonded discs are not as high as those of the other bonded discs for Ag contents of 0 and 25 mol %, at which the dimples were produced.

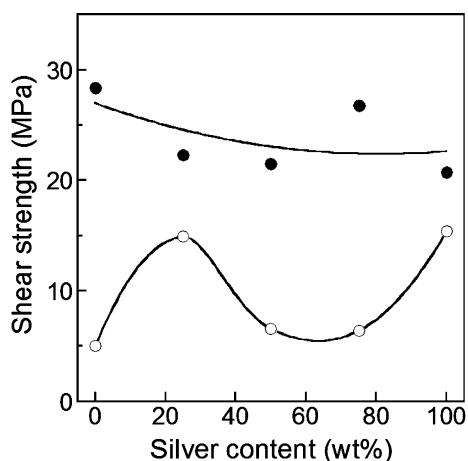


Fig. 9 Shear strengths vs. silver content in silver/copper nanoparticles. The bonding was performed in (filled circle) hydrogen gas and (open circle) nitrogen gas

Bonding in nitrogen gas

Photographs of large copper discs after bonding in nitrogen and measurement of shear strength are shown in Fig. 11. As for the nanoparticles containing copper, the surfaces are dark brown, and the color tones are darker than those of the copper disks bonded in hydrogen. In particular, the tone is the darkest for 0 mol % ($\text{Ag}_0\text{Cu}_{100}$ nanoparticles). These observations indicate that the copper in the nanoparticles is oxidized to a certain extent. As for the silver nanoparticles, some objects with a color of not black but white are present on the surface. This observation implies that the chemical stability of silver makes it possible to form metallic bulk

phase with no oxidation and possibly contributes to bonding of metallic copper discs. Shear strength is plotted against silver content in the nanoparticles in Fig. 9 white dots. At 0 mol %, shear strength is 5.0 MPa, which increases to 14.9 MPa with increasing silver content to 25 mol %. It is noted that the metal–metal bonding in nitrogen gas (in contrast to hydrogen gas) was achieved using the nanoparticles with copper content as high as 75 mol % (silver content of 25 mol %) or using the nanoparticles whose main component was copper. According to the XRD measurements, the copper component formed the silver/copper alloy. The formation of silver/copper alloy is considered to control oxidation of the silver/copper nanoparticles; Silver, which is chemically stable in metallic state, may reduce partially oxidized particle surface. As a result, the copper discs are strongly bonded at 25 mol % of silver with no oxidation. The shear strength decreases to 6.6 and 6.4 MPa when silver content increases to 50 and 75 mol %, respectively. The mismatch in the d values of copper and silver probably deteriorates the bonding of copper. In contrast, shear strength increases to 15.4 MPa when silver content increases to 100 mol %. In spite of the mismatch of d values, the $\text{Ag}_{100}\text{Cu}_0$ nanoparticles showed shear strength of 15.4 MPa. As for strong bonding, the oxidation of copper in the nanoparticles and the mismatch are probably compensated by the chemical stability of silver. SEM images of the surface of the copper stage after the measurement of shear strength are shown in Fig. 12. Sintering of nanoparticles was observed on all the copper-disc surfaces, although dimples were not formed. These observations indicate that the

Fig. 10 SEM images of the copper plates shown in Fig. 8

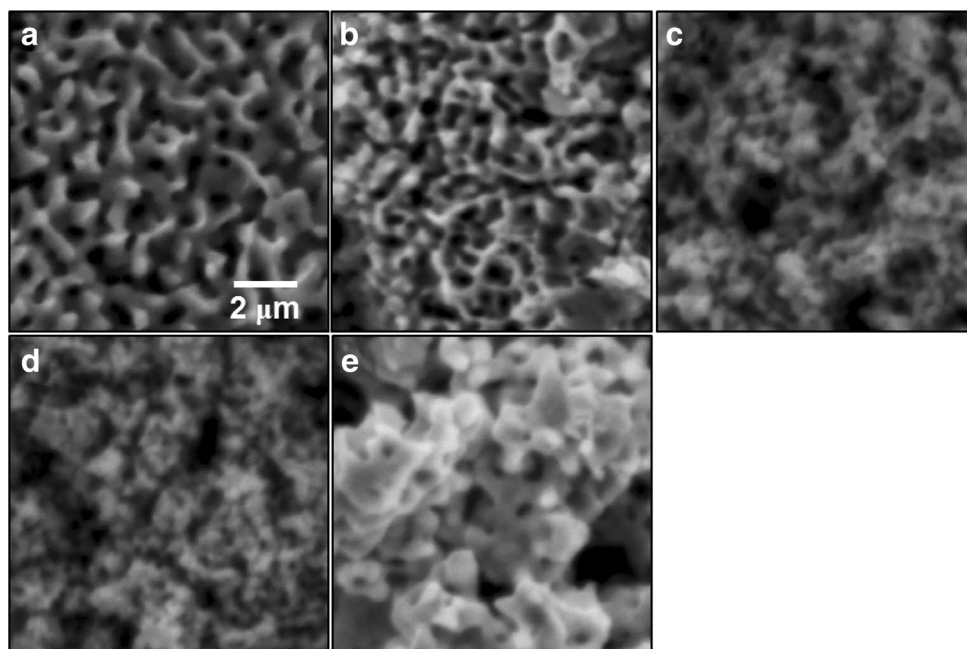


Fig. 11 Photographs of copper plates after measurement of shear strength. The powders used were composed of, **a** $\text{Ag}_0\text{Cu}_{100}$, **b** $\text{Ag}_{25}\text{Cu}_{75}$, **c** $\text{Ag}_{50}\text{Cu}_{50}$, **d** $\text{Ag}_{75}\text{Cu}_{25}$, and **e** $\text{Ag}_{100}\text{Cu}_0$ nanoparticles. The bonding was performed in nitrogen gas

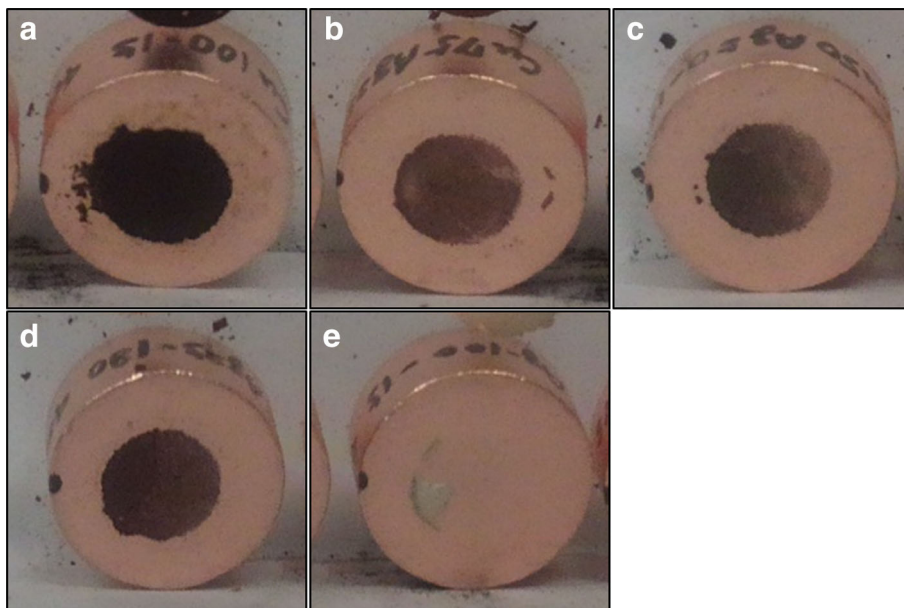
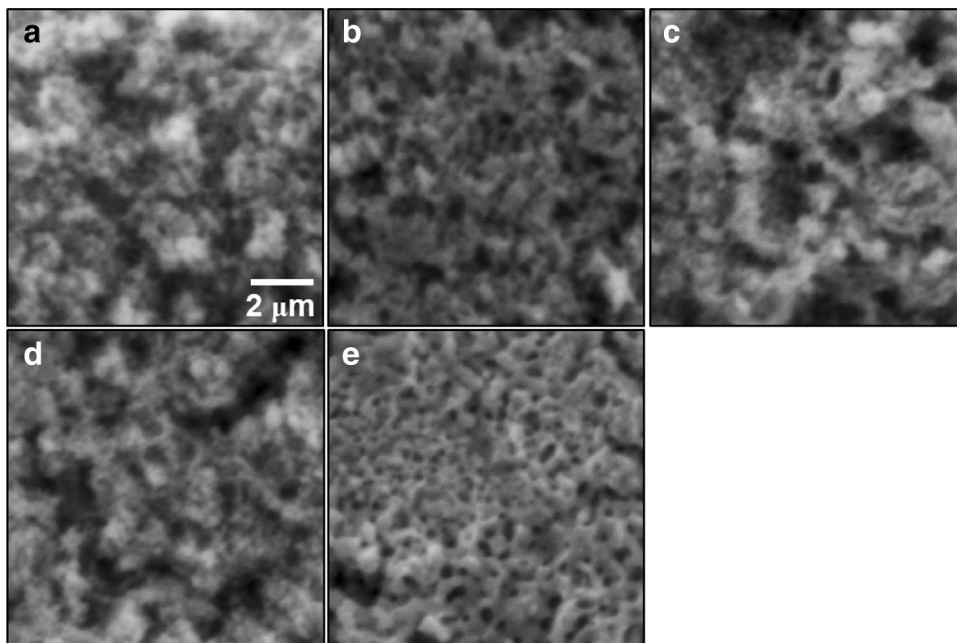


Fig. 12 SEM images of the copper plates shown in Fig. 11



copper discs were adequately bonded, although the shear strengths were lower than those in the case of bonding in hydrogen gas.

Conclusion

Silver/copper nanoparticles composed of metallic copper phase and silver-rich silver/copper phase were synthesized by reducing Ag^+ ions in aqueous solution in the presence of the copper nanoparticles fabricated by reducing CuO

nanoparticles. Silver/copper nanoparticles with average size of 49 nm and crystal size of 16.8 nm were fabricated by adjusting initial concentrations to 0.0075 M Cu^{2+} , 0.0025 M Ag^+ , 1.0 g/L PVP, and 0.6 M hydrazine. XRD measurements indicated the formation of silver/copper alloy phase. XPS measurements revealed that the surfaces of the nanoparticles are slightly oxidized but their bulk is metallic. The silver/copper nanoparticles bond the copper discs bonded when they are pressed between the discs under annealing at 400 °C at 1.2 MPa in not only hydrogen gas but also nitrogen gas. As for the hydrogen gas, a shear

force of 22.3 MPa was required to separate the bonded discs. The shear strength was 14.9 MPa even for nitrogen gas, which is 66.8 % of that for hydrogen gas. The formation of silver/copper alloy is considered to provide successful metal–metal bonding in nitrogen gas.

Acknowledgments This work was partially supported by Hitachi Ltd. We express our thanks to Prof. T. Noguchi in the College of Science of Ibaraki University, Japan (current affiliation: Faculty of Arts and Science of Kyushu University, Japan) for his help with TEM observation.

Open Access This article is distributed under the terms of the Creative Commons Attribution 4.0 International License (<http://creativecommons.org/licenses/by/4.0/>), which permits unrestricted use, distribution, and reproduction in any medium, provided you give appropriate credit to the original author(s) and the source, provide a link to the Creative Commons license, and indicate if changes were made.

References

- Basaran C, Jiang J (2002) Measuring intrinsic elastic modulus of Pb/Sn solder alloys. *Mech Mater* 34:349–362
- Belyakov SA, Gourlay CM (2015) Metastable in Pb-free joints between Sn-3.5Ag and Ni-based substrates. *Mater Lett* 148:91–95
- Chen X, Xue F, Zhou J, Yao Y (2015) Effect of In on microstructure, thermodynamic characteristic and mechanical properties of Sn-Bi based lead-free solder. *J Alloys Compd* 633:377–383
- Daly AAE, Desoky WM, Elmosalami TA, Shaarawy MGE, Adbraboh AM (2015) Microstructural modifications and properties of SiC nanoparticles-reinforced Sn-3.0Ag-0.5Cu solder alloy. *Mater Des* 65:1196–1204
- Das A, Ghosh MM (2015) MD simulation-based study on the melting and thermal expansion behaviors of nanoparticles under heat load. *Comput Mater Sci* 101:88–95
- Gao XY, Wang SY, Li J, Zheng YX, Zhang RJ, Zhou P, Yang YM, Chen LY (2004) Study of structure and optical properties of silver oxide films by ellipsometry. XRD and XPS methods. *Thin Solid Films* 455–456:438–442
- Ghodselaheh T, Vesaghi MA, Shafiekhani A, Baghizadeh A, Lameii M (2008) XPS study of the Cu@Cu₂O core-shell nanoparticles. *Appl Surf Sci* 255:2730–2734
- Gomez J, Basaran C (2006) Damage mechanics constitutive model for Pb/Sn solder joints incorporating nonlinear kinematic hardening and rate dependent effects using a return mapping integration algorithm. *Mech Mater* 38:585–598
- Guo W, Wang L, Zhu Y, Chu PK (2015) Microstructure and mechanical properties of C/C composite/TC4 joint with inactive AgCu filler metal. *Ceram Int* 41:7021–7027
- Iqbal N, Xue P, Wang B, Li Y (2014) On the high strain rate behavior of 63-37 Sn-Pb eutectic solders with temperature effects. *Int J Impact Eng* 74:126–131
- Kanninen P, Johans C, Merta J, Kontturi K (2008) Influence of ligand structure on the stability and oxidation of copper nanoparticles. *J Colloid Interface Sci* 318:88–95
- Kobayashi Y, Maeda T, Watanabe K, Ihara K, Yasuda Y, Morita T (2011) Preparation of CuO nanoparticles by metal salt-base reaction in aqueous solution and their metallic bonding property. *J Nanopart Res* 13:5365–5372
- Kobayashi Y, Shirochi T, Yasuda Y, Morita T (2012) Metal-metal bonding process using metallic copper nanoparticles prepared in aqueous solution. *Int J Adhes Adhes* 33:50–55
- Kobayashi Y, Shirochi T, Maeda T, Yasuda Y, Morita T (2013a) Microstructure of metallic copper nanoparticles/metallic disc interface in metal-metal bonding using them. *Surf Interface Anal* 45:1424–1428
- Kobayashi Y, Shirochi T, Yasuda Y, Morita T (2013b) Synthesis of silver/copper nanoparticles and their metal-metal bonding property. *J Min Metall Sect B* 49:65–70
- Kobayashi Y, Abe Y, Maeda T, Yasuda Y, Morita T (2014) A metal-metal bonding process using metallic copper nanoparticles produced by reduction of copper oxide nanoparticles. *J Mater Res Technol* 3:114–121
- Kotadia HR, Howes PD, Mannan SH (2014) A review: on the development of low melting temperature Pb-free solders. *Microelectron Reliab* 54:1253–1273
- Li WH, Lin PS, Chen CN, Dong TY, Tsai CH, Kung WT, Song JM, Chiu YT, Yang PF (2014) Low-temperature Cu-to-Cu bonding using silver nanoparticles stabilized by saturated dodecanoic acid. *Mater Sci Eng, A* 613:372–378
- Lu S, Xu Z, Zuo R (2014) Comparative study of the effect of domain structures on piezoelectric properties in three typical Pb-free piezoceramics. *Ceram Int* 40:13565–13571
- Luo X, Li C, Yang D, Liu F, Chen Y (2015) Sonochemical synthesis of porous Cu₂O-Cu hollow spheres and their photo-catalysis. *Mater Chem Phys* 151:252–258
- Maeda T, Abe Y, Kobayashi Y, Yasuda Y, Morita T (2012) Synthesis of metallic copper nanoparticles using copper oxide nanoparticles as precursor and their metal-metal bonding properties. *Sci Technol Weld Join* 17:489–494
- Maeda T, Kobayashi Y, Yasuda Y, Morita T (2015) Low-temperature metal-metal bonding process using leaf-like aggregates composed of CuO nanoparticles. *J Chem Eng Jpn* 48:1–6
- Mansikkamäki K, Haapanen U, Johans C, Kontturi K, Valden M (2006) Adsorption of benzotriazole on the surface of copper alloys studied by SECM and XPS. *J Electrochem Soc* 153:B311–B318
- Palacio C, Ocón P, Herrasti P, Diaz D, Arranz A (2003) XPS and ARXPS study of silver underpotential deposition on platinum in acid solution. *J Electroanal Chem* 545:53–58
- Park BK, Kim D, Jeong S, Moon J, Kim JS (2007) Direct writing of copper conductive patterns by ink-jet printing. *Thin Solid Films* 515:7706–7711
- Plackowski C, Hampton MA, Nguyen AV, Bruckard WJ (2013) The effects of X-ray irradiation and temperature on the formation and stability of chemical species on enargite surfaces during XPS. *Miner Eng* 45:59–66
- Prieto P, Nistor V, Nouneh K, Oyama M, Lefdil MA, Diaz R (2012) XPS study of silver, nickel and bimetallic silver–nickel nanoparticles prepared by seed-mediated growth. *Appl Surf Sci* 258:8807–8813
- Ren F, Jiang CZ, Chen HB, Shi Y, Liu C, Wang JB (2004) Metal alloy and mono-elemental nanoclusters in silica formed by sequential ion implantation and annealing in selected atmosphere. *Phys B* 353:92–97
- Rödel J, Webber KG, Dittmer R, Jo W, Kimura M, Damjanovic D (2015) Transferring lead-free piezoelectric ceramics into application. *J Eur Ceram Soc* 35:1659–1681
- Sun PL, Wu SP, Chin TS (2015) Melting point depression of tin nanoparticles embedded in a stable alpha-alumina matrix fabricated by ball milling. *Mater Lett* 144:142–145
- Tyler DR (2015) Metal–metal bond photochemistry as a tool for understanding the photochemical degradation of plastics. *Inorg Chim Acta* 424:29–37

- Yan J, Zou G, Zhang Y, Li J, Liu L, Wu A, Zhou YN (2013) Metal–metal bonding process using Cu+Ag mixed nanoparticles. *Mater Trans* 54:879–883
- Yasuda Y, Ide E, Morita T (2009) Low-temperature bonding using silver nanoparticles stabilized by short-chain alkylamines. *Jpn J Appl Phys* 48:125004–1–125004-5
- Yu CY, Chen WY, Duh JG (2014) Improving the impact toughness of Sn-Ag-Cu/Cu-Zn Pb-free solder joints under high speed shear testing. *J Alloys Compd* 586:633–638